Mathematical Modeling of Biofilm Structure with a Hybrid Differential-Discrete Cellular Automaton Approach

Cristian Picioreanu, Mark C. M. van Loosdrecht, Joseph J. Heijnen

Delft University of Technology, Department of Biochemical Engineering, Kluyver Laboratory for Biotechnology, Julianalaan 67, 2628 BC Delft, The Netherlands; telephone: +31 15 2781551; fax: +31 15 2782355; e-mail: C.Picioreanu@stm.tudelft.nl

Received 8 July 1997; accepted 10 October 1997

Abstract: A hybrid differential-discrete mathematical model has been used to simulate biofilm structures (surface shape, roughness, porosity) as a result of microbial growth in different environmental conditions. In this study, quantitative two- and three-dimensional models were evaluated by introducing statistical measures to characterize the complete biofilm structure, both the surface structure and volume structure. The surface enlargement, coefficient of roughness, fractal dimension of surface, biofilm compactness, and solids hold-up were found to be good measures of biofilm structure complexity. Among many possible factors affecting the biofilm structure, the influence of biomass growth in relation to the diffusive substrate transport was investigated. Porous biofilms, with many channels and voids between the ''finger-like'' or ''mushroom'' outgrowth, were obtained in a substrate-transport-limited regime. Conversely, compact and dense biofilms occurred in systems limited by the biomass growth rate and not by the substrate transfer rate. The surface complexity measures (enlargement, roughness, fractal dimension) all increased with increased transport limitation, whereas the volume measures (compactness, solid hold-up) decreased, showing the change from a compact and dense to a highly porous and open biofilm. *Biotechnol Bioeng* **58:** 101–116, 1998.
Keywords: biofilm; structure; shape; surface; cellular automata; discrete; modeling; roughness; fractal

INTRODUCTION

The morphological characteristics of biofilms (biofilm thickness, biofilm density, and biofilm surface shape) are very important for the stability and performance of a biofilm reactor. Intensive research in the past has revealed a wide variety in biofilm structure, but the relationship between environmental conditions and biofilm structure has not been considered theoretically. For aerobic processes a small biofilm thickness (<150 μm) is favorable due to the smaller diffusional resistance (Tijhuis et al., 1994) and, moreover, because thicker biofilms are sensitive to sloughing phenomena. The control and therefore understanding of biofilm thickness and structure is then an important aspect for a stable operation of biofilm processes. Biofilm surface shape is also an important parameter for the stability of the reactor. These factors also affect considerably the biomass hold-up and mass transfer in a biofilm reactor (Garrido et al., 1997). Especially in particle biofilm processes (e.g., fluidized bed reactors or airlift reactors) fluffy biofilms and outgrowth lead to instabilities. However, suspended organic particles in wastewater are filtrated easier by fluffy and porous biofilms. The biofilm density has a direct effect on the achievable biomass concentration in the reactor; therefore, it will directly affect the conversion of substrate. Hence, establishing and modeling the factors that control biofilm thickness, density, and surface shape is important for the overall performance of the reactor.

Biofilms are very heterogeneous systems, containing cells distributed in a nonuniform manner, and polymers. Moreover, a liquid phase exists in the pores and channels developed in the hydrogel matrix. Therefore, to simulate the development of a structurally heterogeneous biofilm, discrete methods such as cellular automata (Toffoli and Margolus, 1987; Wolfram, 1986) are required. No attempts to model biofilm shape, porosity, or density by a discrete method have been made until recently by Wimpenny and Colasanti (1997). They used a cellular automaton approach to model both diffusion and conversion of substrates into bacterial cells. Their results have shown that availability or lack of nutrients in the bacterial microenvironment leads to different biofilm morphology. This model was, however, very similar to the diffusion-limited aggregation models because only growth at the surface (where unoccupied space is available) and not inside the biofilm structure is assumed. The experimental facts, however, clearly show that the pressure generated by in-depth-growing bacteria also leads to expansion of colonies (biofilms expand in three dimensions).

We believe that, for a scale of millimeters, only the solid particle dynamics (bacteria, polymers, carrier) must be modeled in a discrete way, whereas the nutrient field (which

Correspondence to: C. Picioreanu
Contract grant sponsor: The Netherlands Organisation for Applied Scientific Research
Contract grant number: 95/638/MEP

 CCC 0006-3592/98/010101-16

overlaps solids) can be solved by using conventional differential equations based on mass balances that contain well-known conversion kinetics and mass transport terms. This leads to faster models for use on common computers, using also a set of widely accepted physical/chemical/biological parameters to describe kinetics and transport (Picioreanu et al., 1997). The idea of combining continuous models with discrete ones has been used recently to describe the development of other complex biological structures: bacterial colonies on agar plates (Ben-Jacob et al., 1994); activated sludge flocs (Takács and Fleit, 1995); accretive growth of corals and marine sponges (Kaandorp, 1994); filamentous fungi pellets (Lejeune and Baron, 1997); and slime mold crawling slugs (Savill and Hogeweg, 1997). However, linking the parameters of discrete models with observable and measurable macroscopic variables is still a difficult task.

In a previous article (Picioreanu et al., 1997) we presented a new differential–discrete approach suitable for modeling immobilized cells growing in a gel matrix. The ability of this model to represent diffusion–conversion–microbial growth systems has been quantitatively proven. Not only can substrate and biomass profiles be calculated accurately but, due to the discrete spreading algorithm, the two-dimensional (2D) or three-dimensional (3D) spatial distribution of biomass can also be determined.

In this article, the model is applied to simulate growth of biofilms attached on solid flat surfaces. The biofilm structure, including shape, porosity, and density is generated by the model, unlike in the standard differential models where all these properties are given as input data. In this way we expect to find a model-based explanation for the different biofilm structures experimentally observed under different growth conditions (Kwok et al., 1997) and to check the hypothesis proposed by van Loosdrecht et al. (1995, 1997): ''The biofilm structure is determined by the ratio between detachment forces and biomass production rate in the biofilm.'' Unlike Wimpenny and Colasanti (1997), we believe that not only the variation of substrate concentration in the liquid, but in general the balance between nutrients uptake, their conversion into biomass, then subsequent biomass detachment generates different biofilm structures (van Loosdrecht et al., 1995, 1997). Moreover, we propose a few dimensionless numbers (ratios of relevant process rates) that can be used in relating biofilm structures to different environmental conditions. Among the many possible factors responsible for biofilm structure, only the substrate conversion/transport rate ratio will be studied in the present article, whereas other factors such as bacterial detachment due to shear or sloughing, carrier surface roughness, distribution of bacteria initially attached, or the role of extracellular polymers will be presented in a forthcoming article.

SYSTEM DEFINITION

The general characteristics of the model approach were described in detail previously (Picioreanu et al., 1997). For the case of biofilm formation on solid support only the new assumptions that have been made will be presented. Although both two- and three-dimensional models were made, only the general 3D case is explained in this section. The parameters used in the simulations are presented in Table I.

Space, Variables, and Rules

Biofilm formation is simulated in a Cartesian space with the size of a few hundred microns (see Fig. 1). The length,

Table I. Model parameters.

Parameter	Symbol	Value		Units
		2D	3D	
System dimensions				
Length	l_X	$2 \cdot 10^{-3}$	$0.8 \cdot 10^{-3}$	m
Height	l_Z	$0.4 \cdot 10^{-3}$	$0.32 \cdot 10^{-3}$	m
Width	l_Y	—	$0.4 \cdot 10^{-3}$	m
Grid dimensions				
Length	N	500	200	—
Height	L	100	80	—
Width	M	—	100	—
Substrate (O_2) concentration in bulk liquid	c_{S0}	Variable around $4 \cdot 10^{-3}$ to change G		$kg_S\ m^{-3}$
Initial number of volume elements containing biomass	n_0	250	4000	—
Fraction from the maximum biomass density initially placed in inoculated elements	f	Random distribution between 0.5 and 1		—
Maximum specific growth rate	μ_m	$1.52 \cdot 10^{-5}$		s^{-1}
Growth yield on substrate	Y_{XS}	0.045		$kg_X\ kg_S^{-1}$
Monod saturation constant	K_S	$3.5 \cdot 10^{-4}$		$kg_S\ m^{-3}$
Maintenance coefficient	m_S	$3 \cdot 10^{-5}$		$kg_S\ kg_X^{-1}\ s^{-1}$
Maximum biomass concentration	c_{Xm}	70		$kg_X\ m^{-3}$
Diffusion coefficient	D_S	$1.6 \cdot 10^{-9}$		$m^2\ s^{-1}$
Thickness of diffusive boundary layer	l_b	$40 \cdot 10^{-6}$		m

width, and height of the system are l_X, l_Y, and l_Z, respectively. When a rectangular mesh with $N \times M \times L$ computational elements, $\Omega_{X,Y,Z}$, numbered from 0 to $N-1$, $M-1$, and $L-1$, respectively, is used to discretize the space, we obtain an array of rectangular volume elements each with size $\delta x \delta y \delta z$.

The variables chosen to represent the biofilm state in the simplest case are the dimensionless concentration of a soluble limiting substrate (S) and the biomass density in each element (C). In a third matrix, **c,** we store information about the occupation of space with solid particles (i.e., bacteria, carrier, etc.). A flat plate is placed at the bottom of the work-volume. On this solid support, a number (n_0) of inoculum colonies is initially distributed at randomly chosen positions. The soluble substrate (nutrient) comes from an ideal source situated at the top of the system. We assume, in this work, that biofilm grows in a static liquid environment; that is, the substrate is transferred only by diffusion from the ideal source, through the liquid boundary layer, to the attached bacteria, which consume it. The spatial distribution of substrate is calculated by applying relaxation methods to the reaction–diffusion mass balance. The biomass density map results from direct integration in each grid cell of a substrate-limited growth equation with biomass decay. Spreading of biomass is modeled by a discrete cellular automaton (CA) algorithm, each time the biomass density in a grid element reaches its maximum value, c_{Xm} (Picioreanu et al., 1997).

Boundary Conditions

1. An ideal linear (2D model) or planar (3D model) source of substrate is placed in all computational elements situated at a certain position, Z_b, of the work-volume, meaning that the fixed-value boundary condition, $S_{X,Y,Z} = 1$, stands for any grid element at $(X,Y,Z) \in (0 \ldots N-1, 0 \ldots M-1, Z_b)$. To keep a rather constant external mass transfer resistance, the height at which the source is placed, Z_b, is always at the same fixed distance above the top of the biofilm, Z_{max} (Fig. 1). Thus, the source of substrate (that can be seen as the infinite reservoir of the bulk liquid) will move upward in time while the biofilm front advances (the solid structure grows). Spatial substrate distribution at each time will then be calculated only in the volume under $Z_b(t)$. In the case presented here, we assume a typical external mass transfer coefficient for oxygen, $k_L = 4 \cdot 10^{-5}$ m s^{-1} (de Beer et al., 1994), a value that leads to a boundary layer thickness, $l_b = D_S/k_L = 40$ μm (expressed in grid units, $Z_b - Z_{max} = 10$ elements for the discretization used; see Table I).
2. The zero-flux boundary condition ($dS/dZ = 0$) is assumed at the solid wall on the bottom. The finite difference approximation of the substrate balance equation at a point $(X,Y,1)$ adjacent to the solid boundary is:

$$\frac{S_{X+1,Y,1} - 2S_{X,Y,1} + S_{X-1,Y,1}}{(\delta X)^2} + \frac{S_{X,Y+1,1} - 2S_{X,Y,1} + S_{X,Y-1,1}}{(\delta Y)^2} + \frac{2S_{X,Y,2} - S_{X,Y,1}}{(\delta Z)^2} - \rho(C_{X,Y,1}, S_{X,Y,1}) = 0 \quad (1)$$

   In the case of a rough carrier, the diffusional terms are correspondingly modified to take into account the zero gradient of concentration at the solid boundary.
3. A periodic (cyclic) boundary condition is built in the X direction (at the left and right sides) and Y direction (near and far faces of the volume). Sides 1 with 2 and 3 with 4, respectively (Fig. 1), are connected to realize the ''periodic space,'' which can diminish the effects of the finite size of the lattice. For example, the periodic boundary condition implemented in the X direction means that each grid element at $X = N-1$ has, as nearest neighbor, an element at $X = 0$ sharing the same Y and Z coordinates. As a direct implication, the new biomass that has to be redistributed from the element $(N-1, Y,Z)$ to the positive X direction will go in the element $(0,Y,Z)$. This type of boundary condition in X and Y holds for all **S, C,** and **c.**

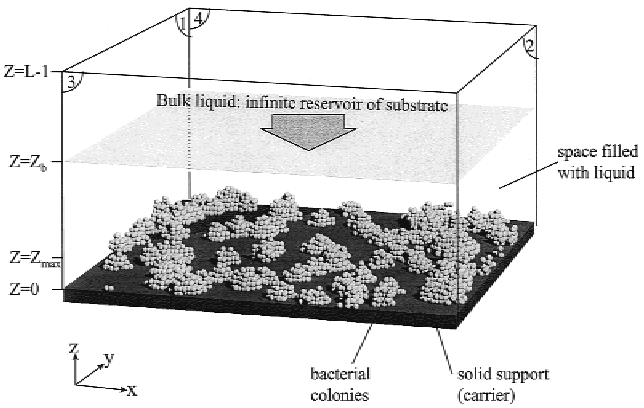

Figure 1. System definition.

CHARACTERISTIC VARIABLES

Measures of shape quantify only the information that remains once location, orientation, and size features of the object have been dealt with (Glasbey and Horgan, 1994). This means that biofilm shape measures must be invariant to the position, size, or orientation of the biofilm. There are very many possibilities for describing shape and the problem is frequently recognized as an open-ended task. Here we will introduce a few selected statistical quantities to characterize the internal and external structure of simulated biofilms.

Because we are interested in studying the formation of biofilm structure, it is useful to define first the *biofilm front,* also referred to in the literature as the ''external perimeter'' or the ''border.'' Similar to the diffusion front introduced by Sapoval et al. (1985) and Chopard and Droz (1990), the biofilm front is constructed as follows:

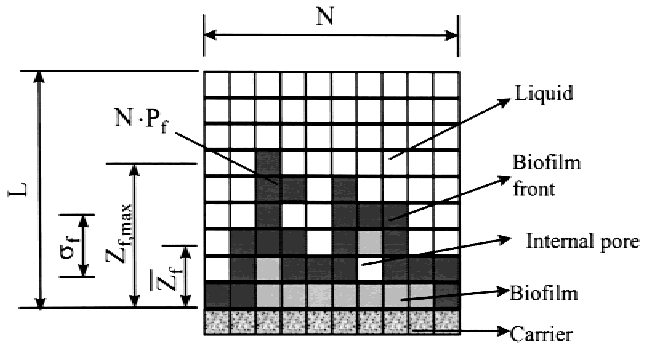

Figure 2. Construction of the biofilm front with nearest and next-nearest liquid boundary (the ''eight neighbors'' case).

1. The first step is to determine the infinite cluster (''the fluid''), consisting of those empty sites connected by the nearest neighbor to the infinite reservoir.
2. The complementary cluster is the biofilm (''the land''), defined as all particles connected to the carrier by nearest-neighbor particle–particle bonds. The biofilm also includes empty sites (pores, voids), which are finite empty clusters (''lakes'').
3. The biofilm front comprises the chain of nearest-neighbor particle–particle bonds in such way that each particle of the hull has at least one ''fluid'' (external) *nearest* or *next-nearest* neighbor (Fig. 2). There are also other possibilities to define the front line. For example, a biofilm front particle is the particle that has external fluid neighbors only in the *nearest* points. In the present study we use only the first option. The variables characterizing the front constructed in another manner will have different values, but the general behavior is the same.

Biofilm Surface Enlargement

The biofilm surface area is an important parameter in the design and performance evaluation of biofilm reactors. This is mainly because it explicitly enters into all mass transfer calculations as the biofilm/liquid interface. Biofilm surface areas are usually calculated in a simple manner, assuming—depending on the carrier used—simple shapes for the biofilm substratum (i.e., flat, spherical, or cylindrical geometry). However, as has been clearly observed in natural systems, the biofilm surface shape can be very complex and quite far from a simple geometry. Therefore, the first measure of biofilm surface structure introduced is the ratio between the real biofilm surface area and the substratum area. We call this ratio *biofilm surface enlargement.*

To calculate surface enlargement, it is first relevant to define, at time *t,* the *average density* of biofilm front points at distance Z from the solid carrier, $\bar{c}_{f,Z}$, which for our discrete system is:

$$\bar{c}_{f,Z} = \frac{1}{N} \cdot \sum_{X=0}^{N-1} c_{f,X,Z} \text{ in 2D and}$$

$$\bar{c}_{f,Z} = \frac{1}{M \cdot N} \cdot \sum_{X=0}^{N-1} \sum_{Y=0}^{M-1} c_{f,X,Y,Z} \text{ in 3D} \quad (2)$$

where $c_{f,X,Y,Z}$ is the state of the occupation matrix: 0 for a nonfront point and 1 for a front point (so that $0 \leq \bar{c}_{f,Z} \leq 1$). To compare the results, it is useful to introduce a *normalized density* of distribution of front points:

$$E_{f,Z} = \frac{\bar{c}_{f,Z}}{\sum_{Z=0}^{L-1} \bar{c}_{f,Z}} \quad (3)$$

Analogous to $\bar{c}_{f,Z}$, the average substrate, $\bar{S}_Z$, and biomass, $\bar{C}_Z$, concentrations and the average space occupation, $\bar{c}_Z$ (a measure of *surface coverage*), are also defined for the slice, Z. These variables will be used later to represent front spreading.

The *front length* is then defined in the discrete system as the number of front points (black grid elements in Fig. 2). Normalization will be made relating this sum to the lattice dimension (N, in 2D) or lattice area $M \times N$ in 3D). The normalized biofilm perimeter (P_f) will be obtained in 2D, whereas in the 3D system it means the normalized biofilm surface area (A_f). This measure, simply called *surface enlargement,* is defined by:

$$P_f = \sum_{Z=0}^{L-1} \bar{c}_{f,Z} = \frac{\sum_{X=0}^{N-1} \sum_{Z=0}^{L-1} c_{f,X,Z}}{N} \text{ in 2D and}$$

$$A_f = \sum_{Z=0}^{L-1} \bar{c}_{f,Z} = \frac{\sum_{X=0}^{N-1} \sum_{Y=0}^{M-1} \sum_{Z=0}^{L-1} c_{f,X,Y,Z}}{M \cdot N} \text{ in 3D} \quad (4)$$

The connection of the front points is only by nearest-neighbor bonds (the first option, Fig. 2).

The surface enlargement coefficient takes usually values greater than 1, meaning that the real surface is increased by some folded structure when compared with the bare surface. Only at short time intervals after surface inoculation are values less than 1 obtained (Fig. 4c,d), which signifies the occurrence of a patchy biofilm (see Fig. 3a, for example).

Biofilm Surface Roughness

The biofilm surface enlargement is a good measure for biofilm front complexity but it cannot take directly into account the depth of biofilm irregularities (roughness). That is why another time-dependent variable must be introduced to measure the biofilm surface roughness. The *average biofilm front width* can be defined as the absolute deviation (σ_f) of biofilm front points ($\bar{c}_{f,Z}$) from the mean front position ($\bar{Z}_f$):

$$\sigma_f = \frac{\sum_{Z=0}^{L-1} |Z - \bar{Z}_f| \cdot \bar{c}_{f,Z}}{\sum_{Z=0}^{L-1} \bar{c}_{f,Z}} \quad (5)$$

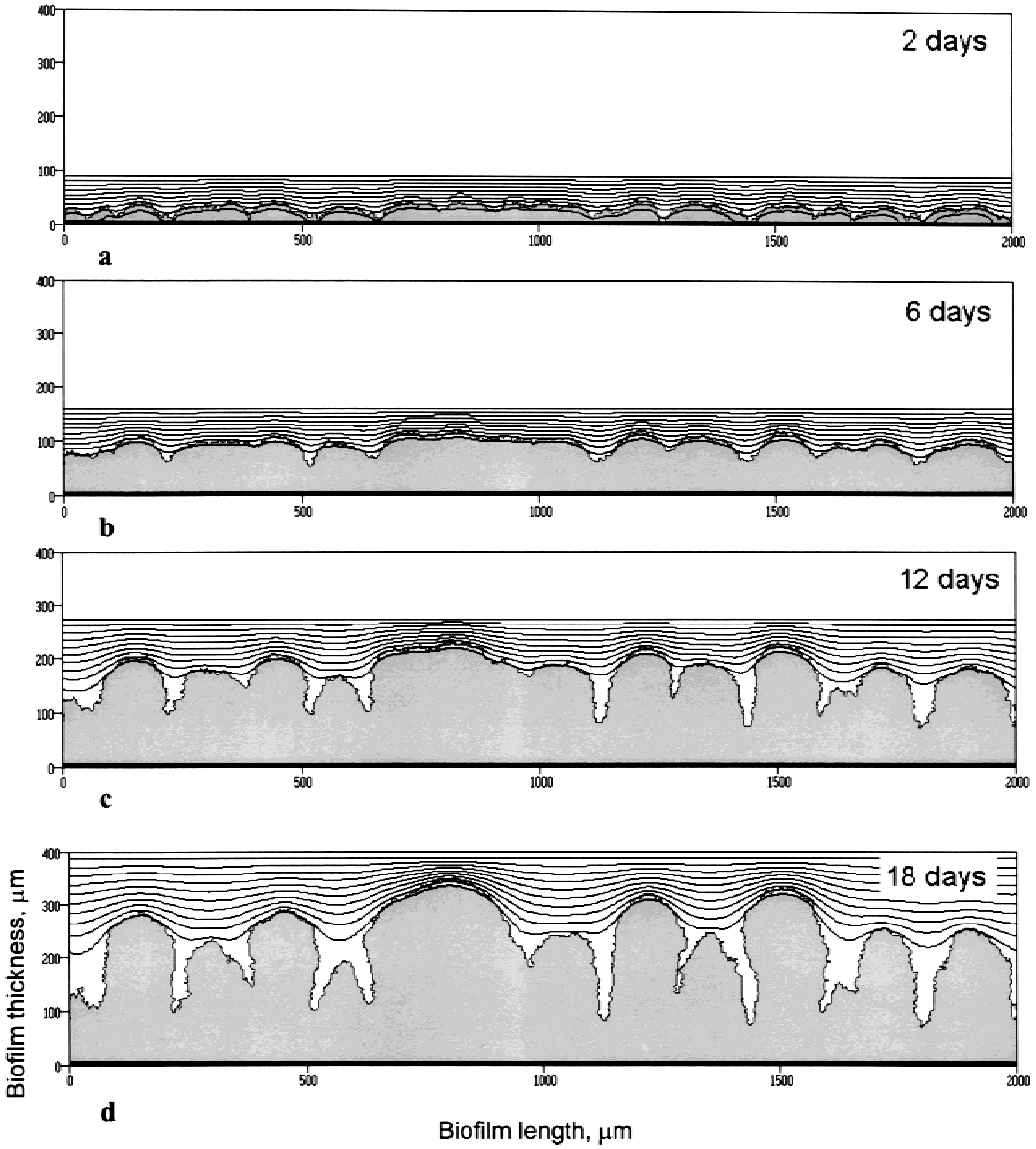

Figure 3. Spatial biomass distribution and lines of equal substrate concentration in a 2D simulation at $G = 10$, after (a) 2, (b) 6, (c) 12, and (d) 18 days. The substrate concentration contour lines are drawn at an interval of 10% from the bulk concentration. On the axes are the length and height of the system in microns.

where the *mean front position* (or the mean of the front-points distribution having, in this case, the signification of the sample *mean thickness*), $\overline{Z}_f$, is the first moment of front-elements distribution in relation to the origin:

$$\overline{Z}_f = \frac{\sum_{Z=0}^{L-1} Z \cdot \overline{c}_{f,Z}}{\sum_{Z=0}^{L-1} \overline{c}_{f,Z}} \tag{6}$$

The absolute deviation, σ_f, depends, however, on the biofilm mean thickness, which was emphasized in Murga et al. (1995). To compare the biofilm roughness obtained in numerical biofilm experiments using different parameters, or at different time intervals, a dimensionless deviation, σ, is defined by relating the average front width to mean biofilm thickness:

$$\sigma = \frac{\sigma_f}{\overline{Z}_f} \tag{7}$$

Like Murga et al. (1995), we call this parameter the *coefficient of surface roughness*. The smaller the σ, the smoother the biofilm surface, whereas a high value of σ means a rough or even patchy biofilm.

Fractal Dimension of Biofilm Surface

In the case of complex structures it is well known that the estimated perimeter grows to infinitely large dimensions as

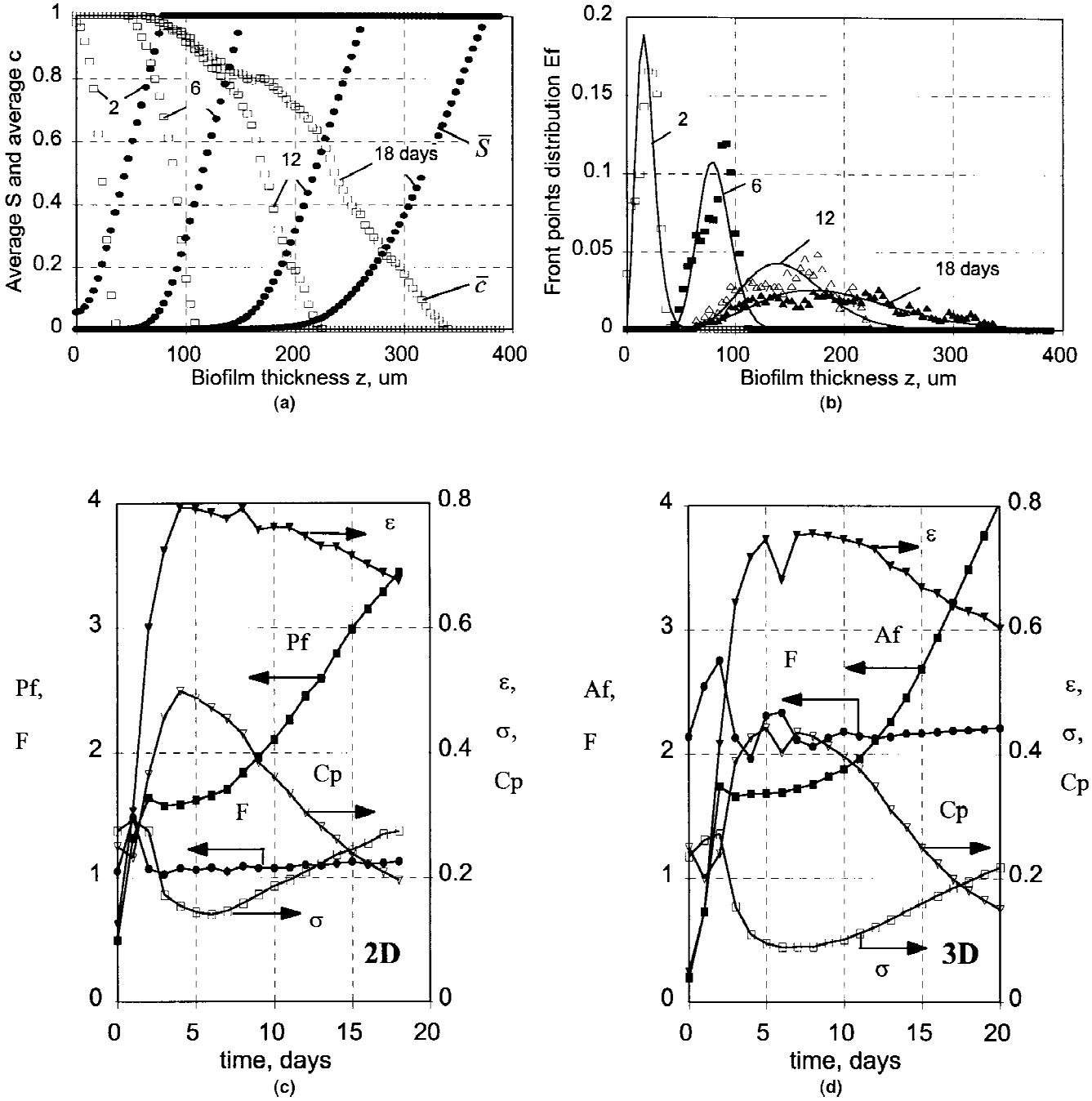

Figure 4. (a) Average dimensionless substrate concentration ($\bar{S}$, ●) and average space occupation ($\bar{c}$, □) profiles along the z-axis after 2, 6, 12, and 18 days at $G = 10$. The graphs correspond to the two-dimensional structures presented in Figures 3a–d. (b) Front-points density distribution, $E_f(Z)$, as a result of 2D simulations after 2 (□), 6 (■), 12 (△), and 18 (▲) days, and curves representing $E_f(Z)$ calculated with a gamma function [eq. (17)]. (c) Variation in time of biofilm characteristics: surface enlargement, P_f (■); roughness coefficient, σ (□); solids hold-up, ε (▼); compactness, C_p (▽); and fractal dimension of biofilm surface, F (●), for the two-dimensional model with $G = 10$. (d) Variation in time of biofilm characteristics: surface enlargement, A_f (■); roughness coefficient, σ (□); solids hold-up, ε (▼); compactness, C_p (▽); and fractal dimension of biofilm surface, F (●), for the three-dimensional model with $G = 10$.

the resolution at which we evaluate the object increases. The ruggedness of the biofilm surface can be therefore described by the *fractal dimension* of the biofilm border (Mandelbrot, 1982). The fractal dimension (F) is an indicator of complexity, with higher values representing objects that have more complex shapes than objects with lower F. Increased complexity is seen here in the form of more convolutions and irregularities along the biofilm–liquid interface. There are now many methods to compute fractal dimensions (Avnir, 1989; Kaye, 1989) and measuring their values for

biological objects is usually done by using image analyzers (see, e.g., Hermanowicz et al., 1995; Li and Ganczarczyk, 1990; Obert et al., 1990; Soddell and Seviour, 1994).

The fractal dimension of biofilms simulated with our model is estimated by the box counting method (Kaye, 1989; Obert et al., 1990). Square grids with varying size of tiles (λ) are placed over the biofilm border (in our case, sizes from 1 to 10 grid elements are used). Then, the number of squares, $N_S(\lambda)$, which contain border points is determined. A plot of $\log(N_S)$ against $\log(\lambda)$ yields a line of slope m from which the fractal dimension can be derived (Kaye, 1989):

$$F = 1 + |m| \tag{8}$$

The fractal dimension of the solid–liquid interface, F, takes values between 1 and 2 for the biofilm front in the 2D model. For the three-dimensional model, F goes to 2 as the biofilm surface is completely flat and to 3 when it is very folded and tends to fill all the available space.

Biofilm Solids Hold-Up

Although biofilm surface enlargement and roughness are useful quantitative measurements to handle biofilm structure, they reflect only the surface complexity. From an engineering point of view, a parameter for average occupation of space with solids (e.g., microorganisms catalyzing the desired reaction) is also needed. If we define the biofilm thickness, Z_{max}, as the distance between the substratum and the outermost cell (Murga et al., 1995), then ''biofilm'' means cell colonies and voids together. A measurement that globally captures internal features of the biofilms is the ratio between the number of grid elements occupied with biomass and the total number of grid elements in the rectangle bounded by the maximum thickness and carrier surface (i.e., $N \cdot Z_{max}$). Therefore, *biofilm solids hold-up* is defined as:

$$\varepsilon = \frac{\sum_{X=0}^{N-1}\sum_{Z=0}^{Z_{max}-1} c_{X,Z}}{N \cdot Z_{max}} \text{ in 2D and } \varepsilon = \frac{\sum_{X=0}^{N-1}\sum_{Y=0}^{M-1}\sum_{Z=0}^{Z_{max}-1} c_{X,Y,Z}}{N \cdot M \cdot Z_{max}} \text{ in 3D} \tag{9}$$

Consequently, porous biofilms will have a low solids hold-up, whereas for dense ones $\varepsilon \to 1$. The biofilm *porosity* is then simply $1 - \varepsilon$.

Biofilm Compactness

The last shape statistic we have used is a measure of compactness. It is usually defined in image analysis as the ratio of the area of an object to the area of a circle with the same perimeter (Glasbey and Horgan, 1994). Because in our case we deal with a flat geometry, we redefine the *biofilm compactness* (C_p) in 2D projections as the biofilm area per area of rectangle having the same perimeter:

$$C_p = \frac{\text{biofilm area}}{Z_{max} \cdot \text{biofilm perimeter}} = \frac{\sum_{X=0}^{N-1}\sum_{Z=0}^{Z_{max}-1} c_{X,Z}}{Z_{max} \cdot N \cdot P_f} \tag{10}$$

Similarly, in 3D, the compactness is the total volume of elements occupied with biomass related to the volume of a parallelepiped having the same area of the top face as the biofilm surface area ($N \cdot M \cdot A_f$). The measure takes its largest value of 1 for a compact and completely flat biofilm. Any departures in the biofilm shape from the flat geometry (such as a rather irregular border versus smooth) will decrease the measured value (Glasbey and Horgan, 1994).

MODEL SYSTEM

Model Description

The system we have chosen to represent by this model is the oxidation of ammonia by a nitrifying biofilm containing only *Nitrosomonas europaea.* The limiting substrate is dissolved oxygen varied between 0.7 and 70 mg $O_2 \cdot L^{-1}$ in the bulk liquid. Monod kinetics with a maintenance term is assumed for the oxygen conversion rate, while a decay term is included together with the saturation kinetics of microbial growth (Picioreanu et al., 1997; Wijffels, 1994). All kinetics and stoichiometry of microbial growth as well as oxygen mass transfer parameters (Table I) are taken from Wijffels (1994).

Model Parameters and Dimensionless Numbers

Growth of bacterial colonies in biofilms is the result of substrate conversion into biomass. Because, in the present model, the limiting nutrient is transported from the bulk liquid to the cells only by diffusion, as a result of external and internal mass transfer resistance, a gradient of substrate will form. Each microbial cell will ''see'' a different environment; that is, bacteria situated on top biofilm layers get more substrate than those living in deeper layers. The lower the substrate transport rate (or higher the consumption rate) the steeper the gradient. We believe, therefore, that the biofilm structure will be determined by dimensionless criteria defined (as in classical chemical reaction engineering) as ratios between the rates of relevant processes (external and internal transport, substrate conversion, biomass growth, biofilm detachment, etc.).

The ratio of biomass growth rate to substrate transport is one of the most important parameters in this system. Because the widely used Thiele modulus, ϕ^2, results directly from the mass balance of substrate in the biofilm, by introducing the dimensionless variables, $S = c_s/c_{s0}$, $C = c_X/c_{Xm}$, $Z = x_i/l_z$ (where x_i is x, y, or z), and $K = K_s/c_{s0}$:

$$\nabla^2 S - \phi^2 \frac{S}{S+K} = 0 \tag{11}$$

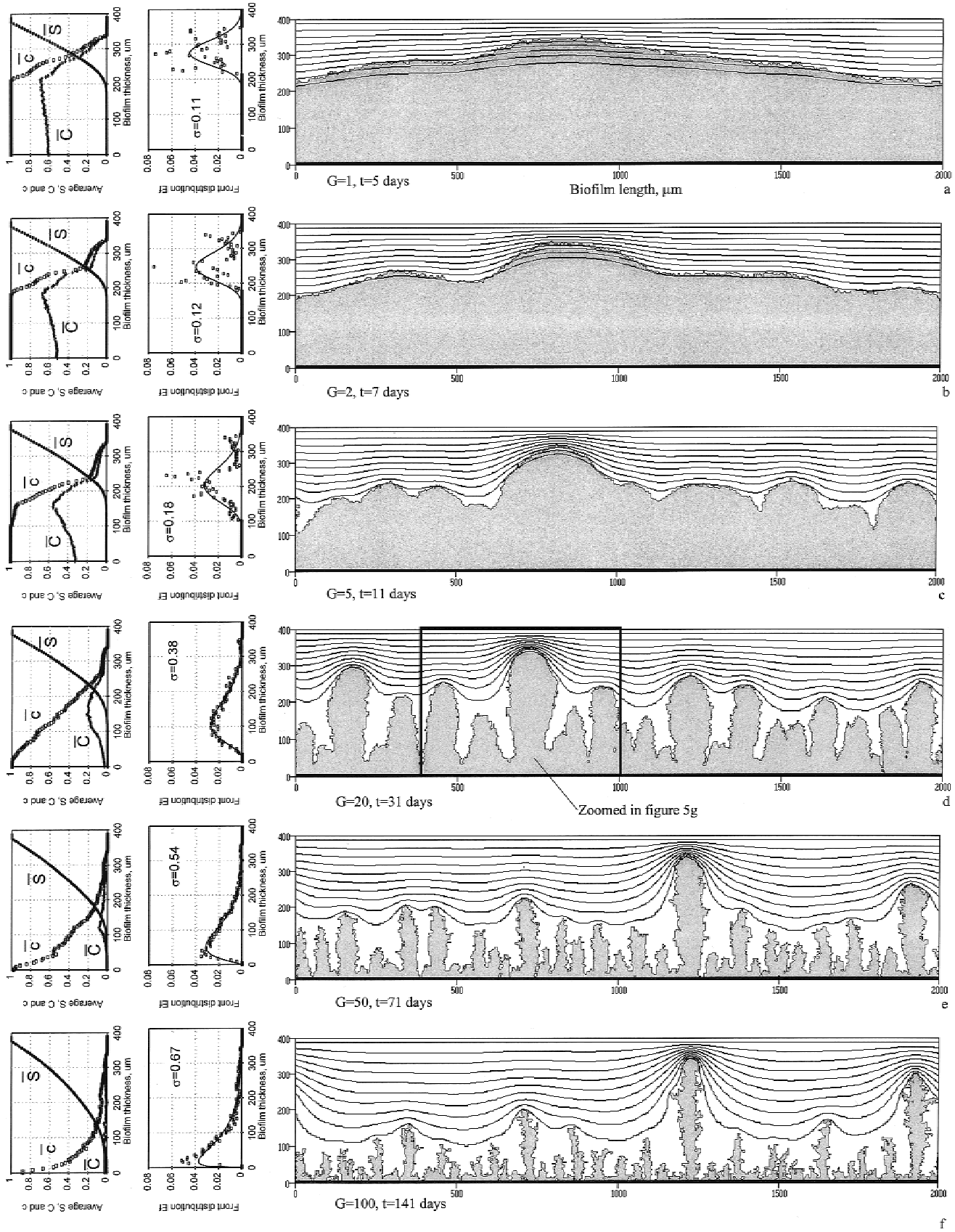

Figure 5. Spatial biomass distribution and lines of equal substrate concentration in 2D simulations at G equal to (a) 1, (b) 2, (c) 5, (d) 20, (e) 50, and (f) 100. Between two adjacent substrate contour lines there is a 10% difference in concentration related to the bulk concentration. All the pictures show the state of the system when a maximum biofilm thickness of 350 μm is reached. (g) Enlarged picture of the vectorial field of concentration gradient (which is proportional to the mass flux transferred to the biofilm) for the region of 400 to 1000 μm in (d). The density of front-point distribution, $E_f(Z)$, as a result of simulation (□) and calculated with a gamma function (lines), is plotted along the biofilm thickness. Roughness coefficient (dimensionless absolute deviation of front-point distribution from the mean thickness) is indicated on graphs. The average dimensionless substrate concentration ($\overline{S}$, ●), biomass density ($\overline{C}$, +), and space occupation with biomass ($\overline{c}$, □) are also represented along the biofilm thickness (z-coordinate).

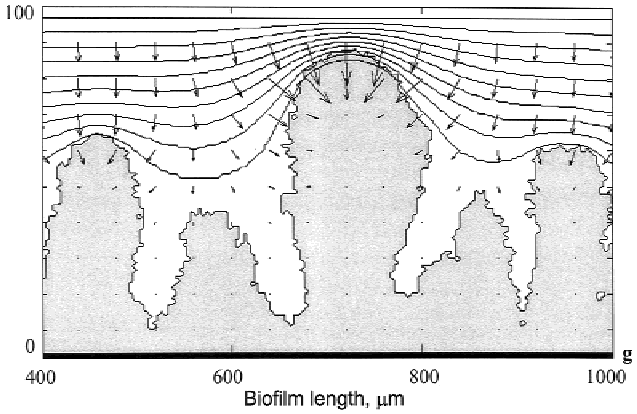

Figure 5. Continued.

$$\phi^2 = \frac{\text{maximum substrate conversion rate}}{\text{maximum substrate transport rate}} = l_z^2 \cdot \frac{q_{Sm} c_{Xm}}{D_S c_{S0}} \tag{12}$$

and by combining ϕ^2 with the biomass growth yield on substrate:

$$Y_{XS} = \frac{\text{maximum biomass growth rate}}{\text{maximum substrate conversion rate}} = \frac{\mu_m c_{Xm}}{q_{sm} c_{Xm}} \tag{13}$$

we can define a new group accounting for biomass growth rate/substrate transport rate:

$$G = \frac{\text{maximum biomass growth rate}}{\text{maximum substrate transport rate}}$$

$$= \phi^2 \cdot Y_{XS} = l_z^2 \cdot \frac{\mu_m c_{Xm}}{D_S c_{S0}} \tag{14}$$

It is clear that the G (growth) group represents, in one parameter, the factors that many researchers have found to affect the biofilm structure: the concentration of soluble nutrient in the bulk, c_{S0}; its diffusion coefficient, D_S; the biomass maximum density in the biofilm, c_{Xm}; the maximum specific microbial growth rate, μ_m; and the biofilm thickness, l_Z. We refer, in what follows, to ''transport limited regime'' when G is high, and ''growth-limited regime'' when G takes low values.

For the simulations we use the parameters given in Table I, and G is varied by changing c_{S0} from low values (transport limited) to high values (growth-limited system).

Also important in this model is the Biot number:

$$Bi = \frac{\text{maximum external substrate transport rate}}{\text{maximum internal substrate transport rate}} = \frac{k_L l_z}{D_S} \tag{15}$$

which is a value that results from the dimensionless equality of substrate fluxes on both sides of the hypothetical plane situated at Z_{max} (the biofilm maximum thickness):

$$Bi \cdot \left(1 - \bar{S}\Big|_{Z_{max}}\right) = \frac{d\bar{S}}{dZ}\Big|_{Z_{max}} \tag{16}$$

When only diffusive transport occurs in the boundary layer, and the effective diffusion coefficient in biofilm is equal to the coefficient in the liquid phase, then the Biot number simply becomes the ratio between the characteristic length of the system and the thickness of the boundary layer, $Bi = l_z/l_b$. In this study, $l_Z = 400$ μm and $l_b = 40$ μm were kept constant and, therefore, the Biot number is constant and takes the value of $Bi = 10$.

Using these dimensionless parameters we can include, in a unifying way, the effects of relevant process rates on biofilm formation and its structural features.

RESULTS AND DISCUSSION

Time Evolution of Biofilm Structure

Figure 3a–d presents the time evolution of a simulated 2D biofilm. Parameters used here are the same as those in Table I, at $G = 10$. It is clear from Figure 3a–d that biofilm complexity increases continuously over time. Initially, the patchy biofilm colonies are completely penetrated by the substrate. They tend to grow in all directions, filling the space existing initially due to the random surface inoculation. As the biofilm thickness grows, some colonies get the chance to be closer to the substrate source than others. These portions of the biofilm experience a higher concentration of nutrients; therefore, new biomass will be formed more quickly, whereas the colonies in the ''valleys'' grow in an environment depleted in substrate. The voids between the colonies cannot be filled with new biomass any longer. The obvious consequence is that a rough, ''finger-like'' biofilm will develop on the top of a compact basal layer.

In Figure 4, a more quantitative evaluation of these observations is offered. The profiles of average substrate concentration ($\bar{S}$, filled circles in Fig. 4a) show a ''penetration depth'' of about 50 μm after 6 days (biofilm top being at 110 μm). Also, the average occupation with solid biomaterial across the biofilm thickness ($\bar{c}_Z$, which can be viewed as the mean surface coverage at a certain biofilm height and is represented by empty squares in Fig. 4a) show that, after a certain time, the compact basal layer (with $\bar{c} \approx 1$) no longer grows. The newly formed biomass extends in a finger-like manner over a larger surface leading to a less dense structure. This effect can be statistically quantified by representing the density of a front-points distribution function, E_f, along the biofilm thickness (Fig. 4b). The initially narrow peak (2 days), meaning a more or less flat biofilm surface, becomes broader in time as the biofilm grows in thickness. The front points spread from an average front width of 40 μm on the second day to about 250 μm after 18 days. It appears that these results obey a gamma distribution; therefore, the computed points are correlated by a gamma (Γ) function having, as parameters, the front-points distribution moments—average front position, $\bar{Z}_f$, and variance, σ_f^2:

$$E_{f,Z} = \frac{\beta^\alpha}{\Gamma(\alpha)} e^{-\beta Z} Z^{\alpha-1} \quad \text{where}$$

$$\alpha = \frac{\bar{Z}_f^2}{\sigma_f^2},\ \beta = \frac{\bar{Z}_f}{\sigma_f^2} \text{ and } \Gamma(\alpha) = \int_0^\infty Z^{\alpha-1} e^{-\alpha} dZ \tag{17}$$

The behavior of the statistic measures we defined for biofilm structure characterization will now be followed in time, for both a 2D (Fig. 4c) and for a 3D model (Fig. 4d), at $G = 10$. Several characteristic regions can be observed in Figure 4c. In the first 3 days the empty spaces between the inoculum cells, initially spread over the surface, are filled with new biomass. There is enough substrate available for all cells growing in this ''colonization age.'' The carrier surface is soon covered with patchy colonies. As a result, the normalized biofilm surface area, P_f (filled squares in Fig. 4c), grows from 0.5 (when the biofilm surface is less than the total carrier area) to 1.6 (when the biofilm surface becomes ''wavy''). There are many gaps between colonies, giving, therefore, an initial surface roughness of $\sigma \approx 0.3$, together with a low compactness, C_p, and solids fraction, ε. If we look at the change of biofilm roughness, σ, in time (empty squares in Fig. 4c), a continuous increase can be seen only after the effects of nonuniform inoculation become less important (after 3 to 5 days). Once the inoculation empty spaces are completely filled, the surface becomes smoother and the biofilm development enters a secondary phase. The biofilm grows continuously in thickness (Fig. 4a), whereas the front enlargement, P_f, and roughness coefficient, σ, are almost constant and low ($P_f \approx 1.5$ to 1.7 and σ around 0.2). The solids hold-up, ε, reaches a plateau, with compactness characterizing the solid structure (a maximum $C_p = 0.5$ occurs, see inverted empty triangles in Fig. 4c). In a third phase, however (after 8 to 10 days), the fragile balance between biomass growth rate and substrate uptake rate is again broken. Small protuberances on the surface again lead to an advantage, with microorganisms placed there growing faster and forming tower-like colonies. The enlargement factor and roughness coefficient seem to follow a linear increase in time, whereas the solids hold-up and compactness factor decrease. The biofilm surface enlargement is determined only by large dominant colonies (Fig. 3d), which grow alone, keeping between them a certain distance dictated by the diffusional substrate limitation. This means that the depth of voids between these tower-like colonies becomes steadily larger. The surface enlargement, P_f, is continuously increasing; for example, after 2 weeks, the biofilm surface area is three times higher than the flat surface of the bare carrier. However, this important increase in the solid–liquid interface does not significantly affect the global mass transfer into the biofilm, because in the absence of convection in voids the amount of substrate that exists there is negligible (see 2D concentration profiles in Fig. 3d). It is then clear that the surface enlargement factor, P_f, the roughness coefficient, σ, the solids hold-up, ε, or compactness, C_p, can be used for characterization of biofilm structure at a certain moment in time. These measure the changes in biofilm complexity already seen by visual observation.

In this simulation, the values of P_f and σ keep increasing while the solids hold-up and compactness are decreasing, mainly because of the absence of a detachment mechanism. In real-life biofilm, detachment will force the biofilm structural parameters into a steady-state value. The effect of detachment (and, in addition, of roughness of the initial surface upon which the organisms are inoculated) will be dealt with in a forthcoming study.

Also of interest is the behavior of the fractal dimension of biofilm surface, F. Both in 2D and 3D simulations, after some oscillations, F reaches a steady state. This means that the time evolution of the simulated biofilm shape does obey some physical rules. The bacterial colonies grow in a certain pattern dictated by the environmental conditions (here the value of the G group). Hence, in the next section, only the influence of the G group on biofilm structure formation will be shown, in a 2D model as well as in 3D systems.

Influence of Microbial Growth Rate/Substrate Transport Rate (G Number) on Biofilm Structure

First, results of the *two-dimensional model* are presented (Fig. 5a–f). To have comparable structures, the figures show the biofilm solid occupation and substrate distribution in space for different G values at moments when maximum biofilm thickness is 350 μm.

At high rates of substrate transfer ($G = 1$ and 2), the biofilm obtained is compact and rather smooth (Fig. 5a and b). The substrate penetrates an important part of the biofilm, allowing a high and more or less uniform microbial growth rate in the whole biofilm. The basal layer is then thick and biomass inside the biofilm has not decayed much (''+'' points in $\overline{S}$, $\overline{C}$, $\overline{c}$–Z graphs). As a measure of biofilm roughness, the dimensionless standard deviation of front points is very low in this case ($\sigma = 0.11$), indicating the absence of large channels together with low front enlargement ($P_f = 1.48$).

When substrate transport rate decreases ($G = 5$) the biofilm surface becomes more irregular (Fig. 5c). Both roughness and surface enlargement are larger than in the previous case (0.18 and 1.9, respectively). The larger the G value, the deeper the channels formed in the biofilm (Fig. 5a–f). This is because substrate penetrates mainly the superficial biofilm layers (Fig. 5d–f), leading to the preferential growth of microorganisms situated on top of the outgrowing filaments. Figure 5g also shows the vectors ''gradient of concentration,'' which are proportional to the mass fluxes transferred to the biofilm. The flux of limiting substrate is very high at the top of the filaments, but almost no diffusive substrate transfer will be in the biofilm depth. Moreover, the flux will no longer be perpendicular to the substratum, but rather perpendicular to the biofilm front (in agreement with the measured oxygen profiles by de Beer et al., 1994). Hardly any substrate is left for the deeper colonies, which are then starving. As a result, the profiles of biomass concentration along the biofilm thickness here show a maximum; that is, a large decrease on the inside because decay processes are included in the kinetics used, and also a decrease in outer layers due to the decreased occupation of space with biomass (remember that average biomass density at Z was computed globally, counting biomass in both occupied and unoccupied grid elements).

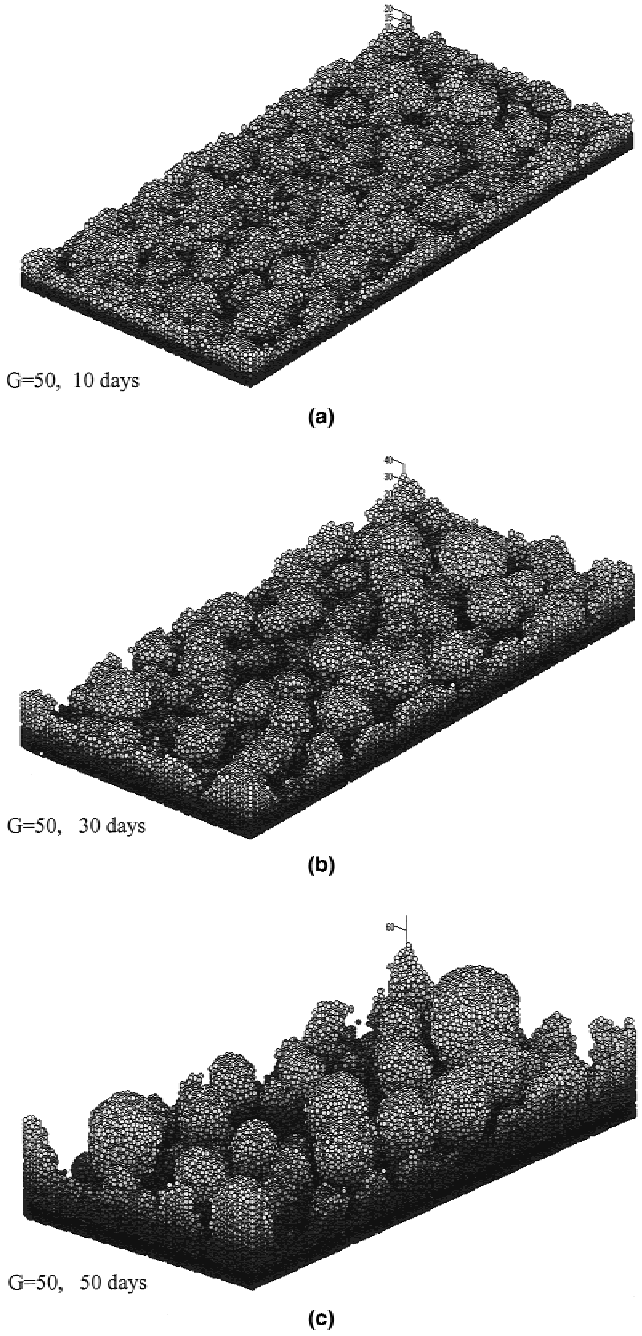

Figure 6. Spatial biomass distribution in a 3D simulation in a substrate-transfer-limited regime ($G = 50$) after (a) 10 days, (b) 30 days, and (c) 50 days. Each circle represents a bacterial cluster with a diameter of 4 μm (the grid size used in simulations).

Very filamentous structures form when substrate is transferred with the lowest rate (G = 100). Biofilm growth is very slow, and a small amount of biomass develops and the structure is very porous (Fig. 5f). Despite the fact that the substrate seems to enter profoundly into the porous biofilm when we look at the average profiles (more than 250 μm from a global thickness of 350 μm), only superficial cells reach it, as we can clearly see in the 2D distribution of substrate (Fig. 5f).

Results obtained with the *three-dimensional model* show the same behavior as the 2D model for G between 1 and 100. Figures 6 and 7 show the biomass spatial distribution for two cases: one at low substrate transfer rate ($G = 50$), and the other one at high rate ($G = 5$). Although both simulations were started with an identical inoculation of the flat surface ($n_0 = 4000$, thus 20% surface coverage), the evolution in time of these two systems is quite different. For a low transfer rate, porous structures are obtained: there are many mushroom-like filaments, while the channels between

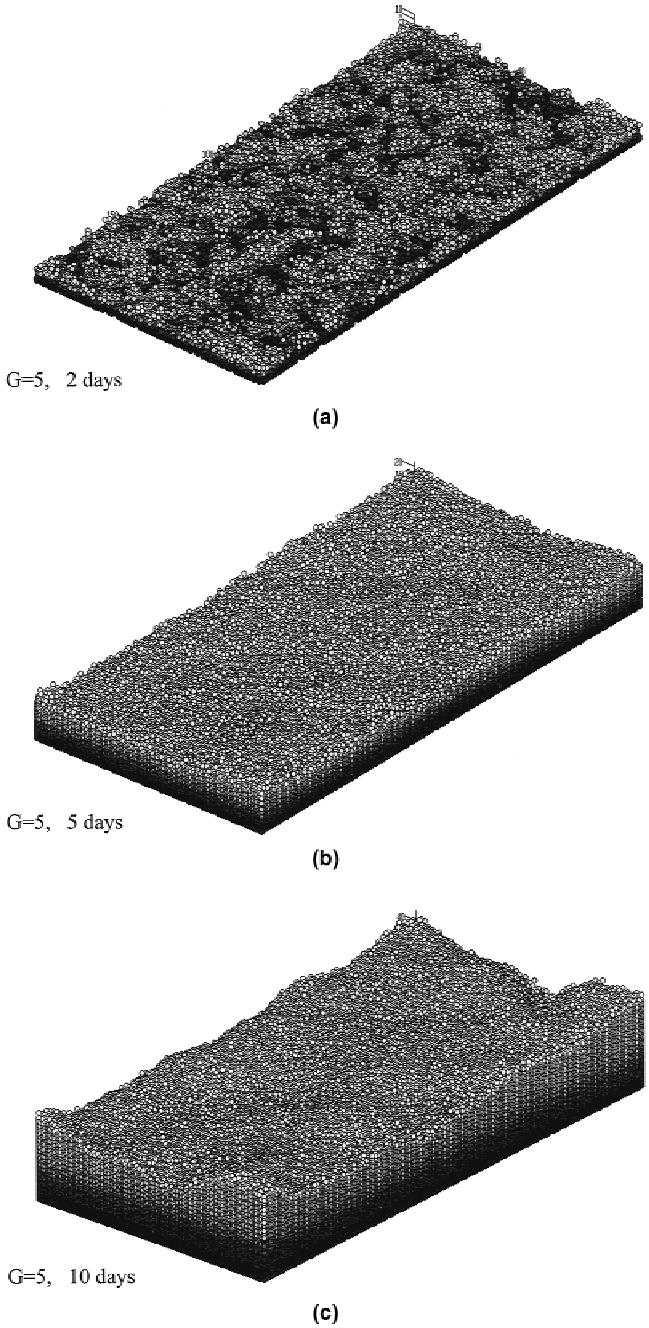

Figure 7. Spatial biomass distribution in a 3D simulation at high substrate transfer rate ($G = 5$) after (a) 2 days, (b) 5 days, and (c) 10 days. Each circle represents a bacterial cluster with a diameter of 4 μm (grid size).

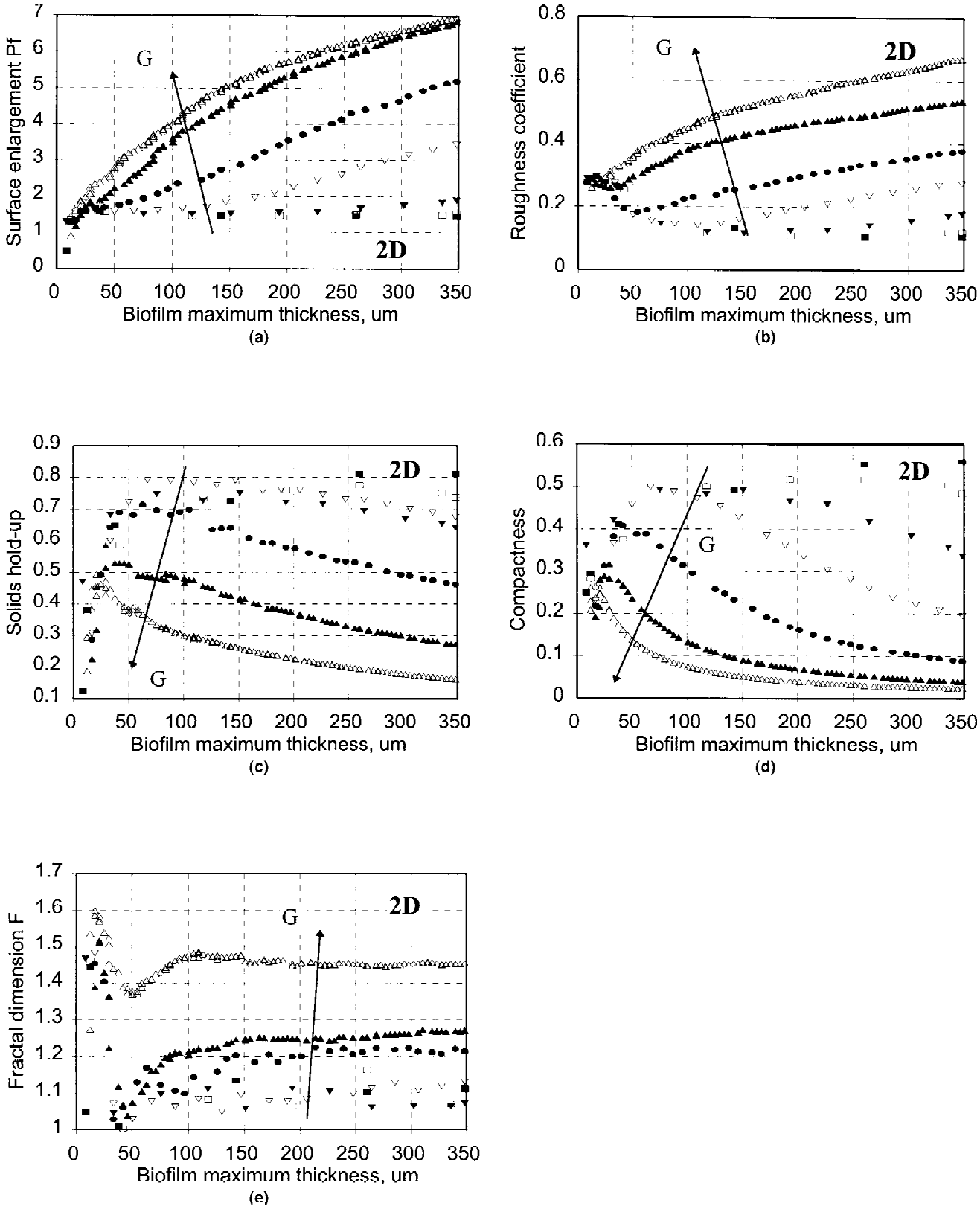

Figure 8. Variation of biofilm structure parameters as a function of *G* group obtained in series of 2D simulations. Symbols on the graphs correspond to *G* values of 1 (■), 2 (□), 5 (▼), 10 (▽), 20 (●), 50 (▲), and 100 (△). Biofilm surface enlargement, P_f (a), biofilm surface roughness, σ (b), solids hold-up, ε (c), biofilm compactness, C_p (d), and fractal dimension of biofilm surface, *F* (e) are plotted against the maximum biofilm thickness (Z_{max}). This was done because the time scale of biofilm development differs very much from low *G* to high *G* values. The time interval between two points in a series is 1 day.

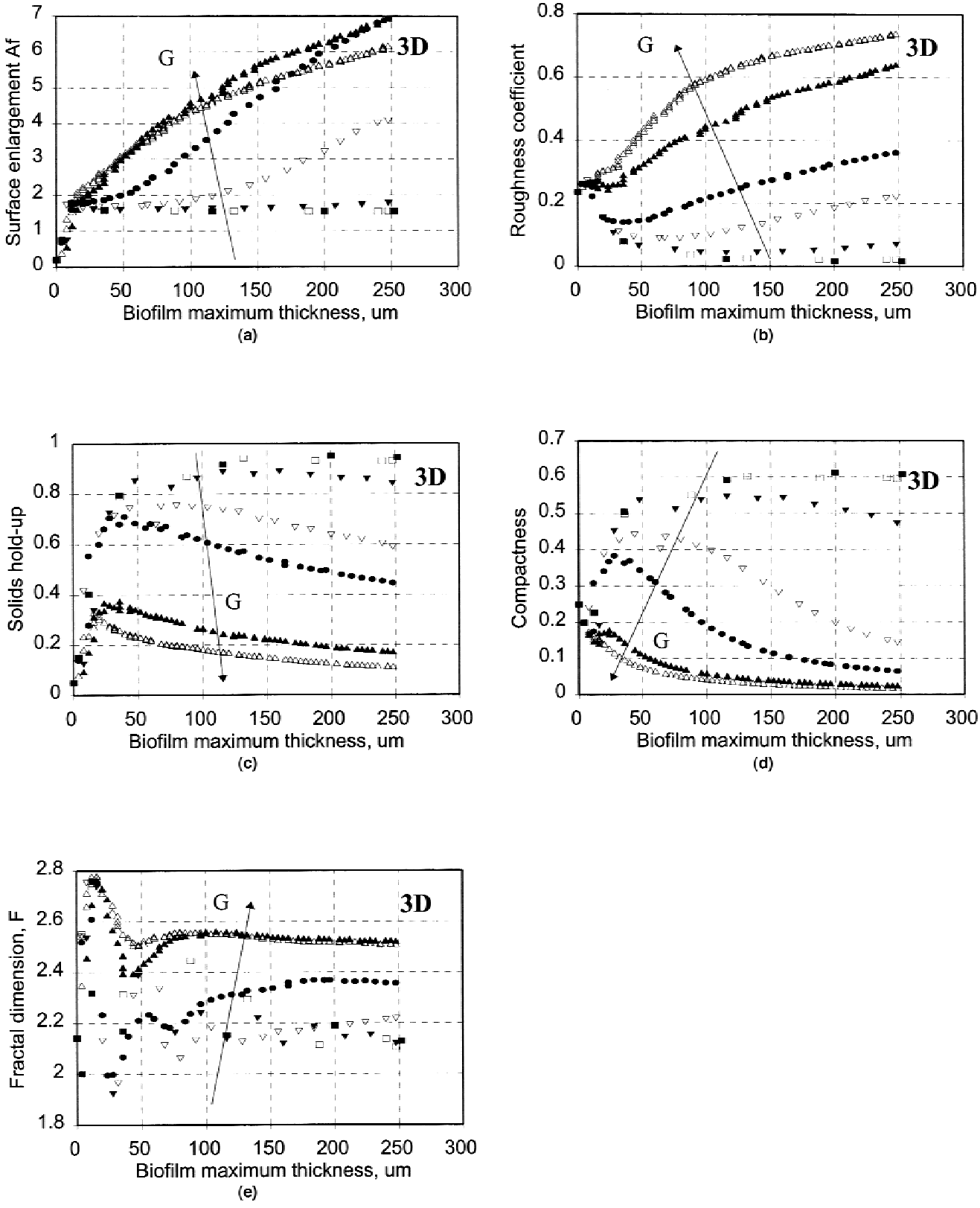

Figure 9. The same variation of biofilm structure parameters as in Figure 8, but obtained in a simulation with the 3D model.

them are very deep (Fig. 6c). When *G* decreases (high substrate transfer rate) the colonies are more compact and the filaments are thicker, until, at the lowest *G,* the resulting structure is very compact (Fig. 7b, c).

Figure 8a–e shows, for the 2D case, how the various measures of biofilm structure change in time. Due to the very different duration needed to obtain the thickness of 350 μm for the different *G* groups applied, we preferred to plot

P_f, σ, ε, C_p, and F as a function of the maximum biofilm thickness reached at a certain time, rather than explicitly use a time abscissa. The values represented by the points in all graphs of Figure 8 were collected at a fixed time interval of 1 day. One can see the same time evolution of biofilm measures as in Figure 4c and d. It happens that, in the first days, the surface roughness (σ) often decreases. This is due to the ''inoculum phase'' described earlier. After a few days (thickness >100 μm), σ and P_f increase linearly (Fig. 8a and b), leading to a constant fractal dimension F (Fig. 8e). It is also of interest to note that there is always a certain biofilm thickness above which the surface protuberances gain a natural advantage, producing a decreased compactness. The lower the G the larger the thickness at which biofilms have maximum compactness; for example, at $G = 2$ this value is around 200 μm, whereas at $G = 20$ it is 30 μm (Fig. 8d). For the 3D case nearly identical characteristic biofilm parameters are found as a function of time (Fig. 9a–e): constant A_f and σ for the growth-limited regime and linear increase for transport-limited regime; stabilization of F; and decrease in compactness and solids hold-up. The amplitude of differences between values obtained at low and high G values obtained at the same maximum thickness (Z_{max}) is, however, higher than in the 2D case (Fig. 9). This is probably due to the greater degree of freedom that cells have in filling a three-dimensional space than in a 2D model.

Figure 10 shows the values obtained at common biofilm thicknesses of 350 μm (2D) or 250 μm (3D case) for characteristic biofilm parameters as a function of the G group (log scale). At a high substrate transfer rate (small G) the biofilm surface is smooth ($\sigma \to 0$) and the interior is compact ($\varepsilon \to 1$, see Fig. 10a, b), leading to a fractal dimension close to 1 (in the 2D case, when the topological dimension of the surface is that of a line) or 2 (the dimension of a planar surface in 3D simulations). As G increases, the surface becomes rough with many protuberances and the volume is less compact ($C_p \to 0$). An increased biofilm surface area is consequently obtained in the transport-limited regime with a higher fractal dimension approaching a superior limit of 1.7 in the 2D model and 2.6 in the 3D model, respectively. Above a certain value of G, however, the number of growing colonies drops, again leading to a significant decrease in P_f and to a maximal F (Fig. 10c, d).

Results presented here were obtained when G was changed by varying the concentration of substrate in the bulk. Another series of simulations, not shown here, in which the diffusion coefficient was modified to give the same G values yielded almost the same values of biofilm

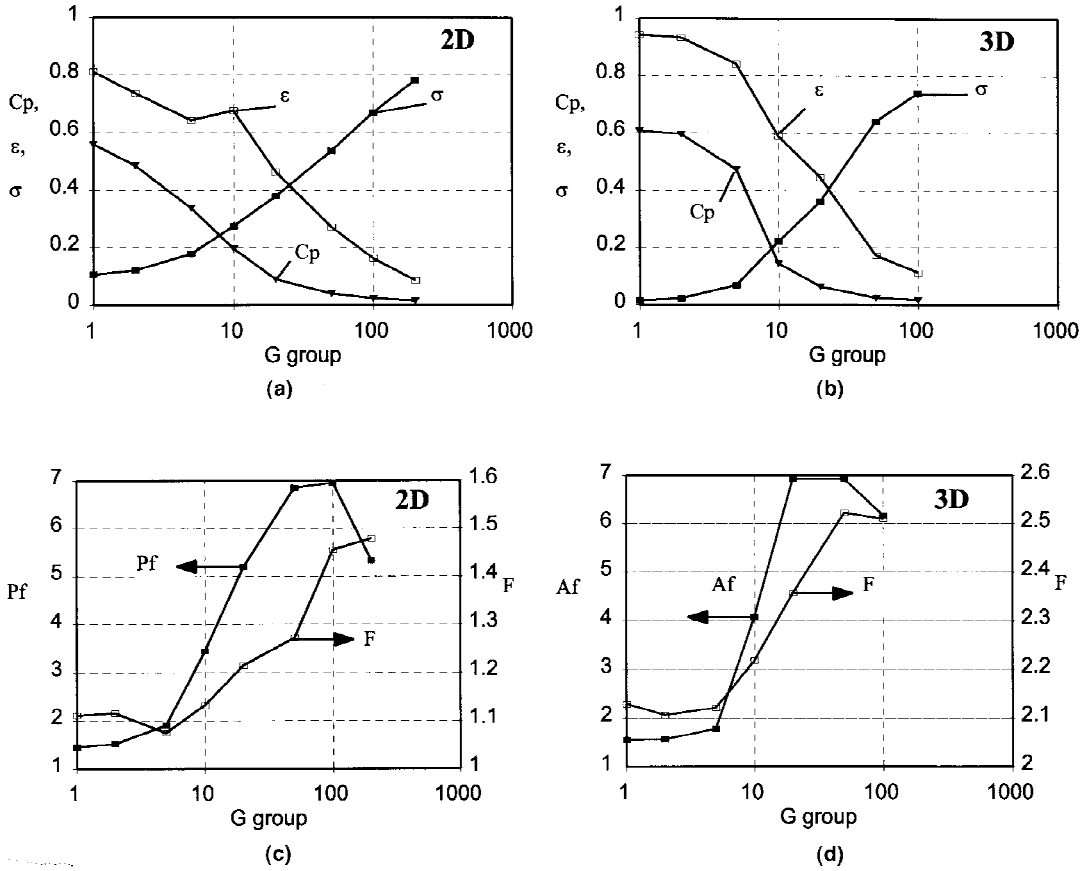

Figure 10. Dependence of characteristic biofilm parameters obtained at the same biofilm thickness (350 μm for the 2D model and 250 μm for the 3D case) as a function of G group. Biofilm solids hold-up, ε (□), roughness coefficient, σ (■), and compactness, C_p (▼) are shown in (a) for 2D and (b) for 3D. Biofilm surface enlargement (■) and fractal dimension (□) are presented in (c) for 2D and (d) for 3D.

characteristics. Only the time scale of biofilm development was affected in latter case. Therefore, we believe that G number groups in a strong correlation some of the factors which clearly affect the biofilm structure, by quantifying the interaction between substrate transport and biomass growth.

CONCLUSIONS

The hybrid discrete-differential approach of biofilm growth described in a previous article (Picioreanu et al., 1997) generated various biofilm structures in different conditions of substrate transport/growth rate. Quantitative two- as well as three-dimensional models have been evaluated in this study. To our knowledge, the proposed model is the first to predict quantitatively the structure of a biofilm from first principles, as a function of environmental conditions.

In this article, only the influence of biomass growth rate/substrate transport rate, the so-called G group, was investigated. Porous biofilms, with many channels and voids, with ''finger-like'' colonies were obtained in a substrate-transfer-limited regime. Compact and dense biofilms resulted at high substrate-transfer rate, and biofilm development was limited only by the growth rate of microorganisms.

Useful statistic variables were introduced to characterize the biofilm structure. The biofilm surface shape was well expressed by the front enlargement, P_f (or A_f), the roughness coefficient, σ, and the fractal dimension, F. Regarding the characterization of biofilm volume, the biofilm solids hold-up, ε, and compactness, C_p, were found to be good measures of biofilm structure complexity. The surface shape measures, σ, P_f (or A_f), and F, all increased smoothly with increasing G, whereas the volume compactness measures, ε and C_p, decreased, showing the change from a compact and dense to a highly porous and open biofilm.

The model presented assumed only microbial growth in a static liquid environment. This is the case that may occur at low bulk liquid velocities, when the boundary layer becomes parallel to the substratum (de Beer et al., 1994). We have shown that even in this simple case a multidimensional model leads to better understanding of biofilm behavior in response to different environmental conditions. Because convective flow is also important, hydrodynamics around the biofilm, together with biomass detachment, will be investigated in a forthcoming study.

NOMENCLATURE

A_f	biofilm front area enlargement (-)
Bi	Biot number (-)
$\bar{c}$	average occupation with biomass (surface coverage) in the slice Z (-)
$\bar{C}$	average dimensionless biomass concentration in the slice Z (-)
c_f	state of occupation matrix indicating front position (0 non-front, 1 front points) (-)
$\bar{c}_{f,Z}$	average density of biofilm front points at distance Z (-)
c_S	substrate concentration ($kg_s\ m^{-3}$)
c_X	biomass density in the biofilm ($kg_x\ m^{-3}$)
c_{S0}	substrate concentration in bulk liquid ($kg_s\ m^{-3}$)
c_{Xm}	maximum biomass concentration in a volume element ($kg_x\ m^{-3}$)
C_p	biofilm compactness (-)
D_s	diffusion coefficient of substrate ($m^2\ s^{-1}$)
$E_{f,Z}$	normalized density of front points distribution (-)
f	fraction from the maximum biomass density initially placed in inoculated grid elements (-)
F	fractal dimension of biofilm surface (-)
G	group accounting for biomass growth rate/substrate consumption rate [defined by eq. (14)] ($kg_x\ kg_s^{-1}$)
k_L	mass transfer coefficient of substrate at the liquid–biofilm interface ($m\ s^{-1}$)
K	dimensionless Monod constant (-)
K_S	Monod saturation constant ($kg_S\ m^{-3}$)
l_b	thickness of diffusive boundary layer (m)
l_X, l_Y, l_Z	length, width, and height of computational space (m)
m_S	maintenance coefficient ($kg_s\ kg_x^{-1}\ s^{-1}$)
N, L, M	grid dimensions (-)
n_0	initial number of volume elements containing biomass (-)
N_S	number of squares containing biofilm front points (-)
P_f	biofilm surface enlargement (-)
q_{Sm}	maximum substrate conversion rate ($kg_s\ kg_x^{-1}\ s^{-1}$)
$\bar{S}$	average dimensionless substrate concentration in the slice Z (-)
t	time (s)
x, y, z	spatial coordinates (m)
X, Y, Z	counters for grid elements in x, y, and z directions (-)
Z_b	thickness of the liquid boundary layer, expressed in number of grid elements (-)
Z_{max}	grid coordinate of the biofilm top (maximum biofilm thickness) (-)
$\bar{Z}_f$	average front position (mean of front points distribution) (-)
Y_{XS}	growth yield on substrate ($kg_x\ kg_s^{-1}$)

Greek symbols

α, β	parameters of gamma distribution function
Γ	gamma integral
ε	biofilm solids hold-up (-)
ϕ^2	Thiele modulus (-)
λ	size of boxes used for determination of the fractal dimension (-)
μ_m	maximum specific growth rate (s^{-1})
σ	biofilm roughness coefficient (the dimensionless absolute deviation of biofilm front points distribution) (-)
σ_f	mean biofilm front width (absolute deviation of biofilm front points distribution) (-)

Matrices

$\mathbf{S}$	matrix of dimensionless substrate concentration distribution in space
$\mathbf{C}$	matrix of dimensionless biomass density distribution in space
$\mathbf{c}$	matrix of space occupation with solids

References

Avnir, D. 1989. The fractal approach to heterogeneous chemistry. John Wiley & Sons, Chichester, UK.

Ben-Jacob, E., Schochet, O., Tenenbaum, A., Cohen, I., Czirók, A., Vicsek, T. 1994. Generic modelling of cooperative growth patterns in bacterial colonies. Nature **368**: 46–49.

Chopard, B., Droz M. 1990. Cellular automata approach to diffusion problems. Springer Proc. Phys. **46**: 130–143.

de Beer, D., Stoodley, P., Roe, F., Lewandowski, Z. 1994. Effects of

biofilm structures on oxygen distribution and mass transport. Biotechnol. Bioeng. **43**: 1131–1138.

Garrido, J. M., van Benthum, W. A. J., van Loosdrecht, M. C. M., Heijnen, J. J. 1997. Influence of dissolved oxygen concentration on nitrite accumulation in a biofilm airlift suspension reactor. Biotechnol. Bioeng. **53**: 168–178.

Glasbey, C. A., Horgan, G. W. 1994. Image analysis for the biological sciences. John Wiley & Sons, Chichester, UK.

Hermanowicz, S. W., Schindler, U., Wilderer, P. 1995. Fractal structure of biofilms: New tools for investigation of morphology. Water Sci. Technol. **32**: 99–105.

Kaye, B. 1989. A random walk through fractal dimensions. VCH, Weinheim, Germany.

Kaandorp, J. A. 1994. Fractal modelling: Growth and form in biology. Springer, Berlin.

Kwok, W. K., Picioreanu, C., Ong, S. L., van Loosdrecht, M. C. M., Ng, W. J., Heijnen, J. J. 1997. Influence of biomass production and detachment forces on biofilm structures in a biofilm airlift suspension reactor. Biotechnol. Bioeng. (accepted for publication).

Lejeune, R., Baron, G. V. 1997. Simulation of growth of a filamentous fungus in three dimensions. Biotechnol. Bioeng. **53**: 139–150.

Li, D., Ganczarczyk, J. 1990. Structure of activated sludge flocs. Biotechnol. Bioeng. **35**: 57–65.

Mandelbrot, B. B. 1982. The fractal geometry of nature. W. H. Freeman, San Francisco, CA.

Murga, R., Stewart, P. S., Daly, D. 1995. Quantitative analysis of biofilm thickness variability. Biotechnol. Bioeng. **45**: 503–510.

Obert, M., Pfeifer, P., Sernetz, M. 1990. Microbial growth patterns described by fractal geometry. J. Bacteriol. **172**: 1180–1185.

Picioreanu, C., van Loosdrecht, M. C. M., Heijnen, J. J. 1997. A new combined differential—discrete cellular automaton approach for biofilm modeling. Biotechnol. Bioeng. **57**: 718–731.

Sapoval, B., Rosso, M., Gouyet, J.-F. 1985. J. Phys. Lett. (Paris) **46**: L149.

Savill, N. J., Hogeweg, P. 1997. Modelling morphogenesis: From single cells to crawling slugs. J. Theor. Biol. **184**: 229–235.

Soddell, J. A., Seviour, R. J. 1994. A comparison of methods for determining the fractal dimensions of colonies of filamentous bacteria. Binary **6**: 21–31.

Takács, I., Fleit, E. 1995. Modelling of the micromorphology of the activated sludge floc: Low DO, low F/M bulking. Water Sci. Technol. **31**: 235–243.

Tijhuis, L., van Loosdrecht, M. C. M., Heijnen, J. J. 1994. Formation and growth of heterotrophic aerobic biofilms on small suspended particles in airlift reactors. Biotechnol. Bioeng. **44**: 595–608.

Toffoli T., Margolus N. 1987. Cellular automata machines; a new environment for modelling. MIT Press, Cambridge, MA.

van Loosdrecht, M. C. M., Eikelboom, D., Gjaltema, A., Mulder, A., Tijhuis, L., Heijnen, J. J. 1995. Biofilm structures. Water Sci. Technol. **32**: 235–243.

van Loosdrecht, M. C. M., Picioreanu, C., Heijnen, J. J. 1997. A more unifying hypothesis for the structure of microbial biofilms. FEMS Microb. Ecol. **24**: 181–183.

Wijffels, R. H. 1994. Effect of initial biomass concentration on the growth of immobilized *Nitrosomonas europaea.* Nitrification by immobilized cells. Ph.D. thesis, Wageningen Agricultural University, Wageningen, The Netherlands.

Wimpenny, J. W. T., Colasanti, R. 1997. A unifying hypothesis for the structure of microbial biofilms based on cellular automaton models. FEMS Microb. Ecol. **22**: 1–16.

Wolfram, S. 1986. Theory and applications of cellular automata. World Scientific, Singapore.